Indian Journal of Fibre & Textile Research
Vol. 45, March 2020, pp. 57-64

Physical and chemical characterization of PLA nanofibres and PLA/ZrO_2 mesoporous composites synthesized by air-jet spinning

Emmanuel Alejandro Albanés-Ojeda[1,2], Roxana Marisol Calderón-Olvera[1,2], Manuel García-Hipólito[1], Daniel Chavarría-Bolaños[3], Roberto Vega-Baudrit[4], Marco Antonio Álvarez-Perez[5] & Octavio Alvarez-Fregoso[1, a]

[1]Institute of Materials Research, National Autonomous University of Mexico, External Circuit 04510 Coyoacan, CDMX, Mexico

[2]Postgraduate in Materials Science and Engineering, Postgraduate Circuit, 04510 Coyoacan, CDMX, Mexico

[3]Department of Diagnostic and Surgical Sciences, School of Dentistry, University of Costa Rica, Costa Rica

[4]National Nanotechnology Laboratory, National Center of High Technology, San Jose, Costa Rica

[5]Tissue Bioengineering Laboratory; DEPeI, Faculty of Dentistry, 04510 Coyoacan, CDMX, Mexico

Received 11 December 2017; revised received and accepted 25 July 2018

Polylactic acid with zirconium oxide solution has been deposited by air-jet spinning to obtain a PLA/ZrO_2 composite. Zirconium oxide is obtained by hydrothermal technique and the results indicate that zirconia is nanostructured, mesoporous and thermally stable. The precursor solutions are formed by different amounts of PLA and zirconia. PLA/ZrO_2 composite is formed by nanofibres with a random distribution, non-porous and with diameter of fibres depending of PLA and zirconia concentrations. It is found that the incorporation of zirconia makes the PLA fibres harder, less flexible and mesoporous. However, the thermal properties are not affected by the zirconia incorporation. The findings show that PLA/ZrO_2 composite can be utilized as biomaterial.

Keywords: Air-jet spinning, Mesoporous materials, PLA/ZrO_2 composite, Polylactic acid nanofibres

1 Introduction

Zirconium oxide (ZrO_2) is an amphoteric oxide that could react as either acid or base substances, which could be monoclinic, tetragonal or cubic in its crystalline structure[1-3]. It is widely used in the industry for its excellent physicochemical properties, such as high chemical stability, high mechanical strength, high melting point, large resistance to fracture, high corrosion resistance, low thermal conductivity, ionic conduction and bio inertness[4,5]. It has also been applied as catalytic compound due its high ion exchange ability and redox movement[6,7], oxygen sensor[8, 9], optical filters and thermal-barrier[10-13]. Nanostructured ZrO_2 due to its wide bandgap is considered as an electric insulator and used in the preparation of piezoelectric, electro optic, dielectric, and nanocomposites materials[14-16]. There are several methods for synthesizing ZrO_2 powders such as sol-gel[17,18], sonochemical[19], molten hydroxides method[20], microwave irradiation[21] and hydrothermal synthesis[22-31]. In the present investigation the ZrO_2 was obtained by hydrothermal synthesis.

Polylactic acid (PLA) is a thermoplastic polymer formed by molecules of lactic acid, which are linked by ester bonds. The study on PLA has been of great interest because it has an important biodegradability both in water and CO_2 as well as excellent biocompatibility[32]. Recently, polymer nanofibres are attractive materials for a wide range of application because of their large surface area to volume ratio and the unique nanometer scale architecture. For the production of nanofibres air-jet spinning (AJS) is becoming a versatile and inexpensive fabrication method for industrialization due to its simple mechanism that produces continuous ultrafine polymer fibres[33]. In the present investigation, ZrO_2 nanoparticles have been used to prepare a composite nanofibre of polylactic acid with zirconia (PLA/ZrO_2) by AJS. In the literature, there are many studies on composites formed by a polymer and a ceramic, such as hydroxyapatite/PLA composites, which have applications in biomaterials[34-36]. However, to the best of our knowledge, no studies have been reported on PLA and nanostructured mesoporous zirconia. Due to the similar properties of zirconia with the hydroxyapatite, it is found interesting to study

[a]Corresponding author.
E-mail: oaf@unam.mx

PLA/ZrO_2 composite properties for application as cell scaffold, adsorption- release of antibiotic materials and catalytic compound. It has been aimed to study the affect of zirconia nanoparticles on PLA fibres, comparing the mechanical properties, wettability, thermal properties and size diameter between pure PLA nanofibres and PLA/ZrO_2 composites.

2 Materials and Methods

2.1 Materials

Sodium hydroxide (NaOH) and zirconyl chloride octahydrate ($Cl_2OZr.8H_2O$), procured from J.T. Baker were used for zirconium oxide synthesis. Polylactic acid ($C_3H_6O_3$; MW = 192,000, named Ingeo 2003D) by Promaplast, Mexico and chloroform ($CHCl_3$) and ethyl alcohol absolute anhydrous (CH_3CH_2OH) by J.T. Baker, were used to process the scaffolds.

2.2 Synthesis of Nanoparticles of Zirconium Oxide

Zirconium oxide was obtained by hydrothermal technique. The volume ratio of zirconyl chloride octahydrate/sodium hydroxide was 3:1. The mixture was allowed to settle over 20 h until a substitution reaction starts between sodium hydroxide and the zirconyl chloride octahydrate to obtain aqueous sodium chloride and zirconium hydroxide as products. These products were rinsed with deionized water for about five times. At the end of all cleaning process, the aqueous zirconium hydroxide (20 mL) was extracted and then kept in an autoclave. Afterwards, the autoclave was placed in a furnace (Barnstead model 1500), heated at 200 °C for 2 h and then cooled at 25 °C. The resultant powder was then dried at 150 °C temperature and crushed in an agate mortar.

2.3 PLA and PLA/ZrO_2 Synthesis

Three polymeric solutions (6, 8, and 10 wt%) of PLA were prepared. PLA (6 wt%) was dissolved in chloroform, stirred the mixture over a day, added ethyl alcohol and stirred again over 20 min to obtain a homogeneous solution. The same process was followed for 8 and 10 wt% of PLA solutions. The volume ratio of chloroform/ethanol was kept 3:1 for all samples.

For PLA with zirconia composites, the same procedure was followed, but at the time of dissolving PLA the nanoparticles of ZrO_2 were also added, using the ratio of PLA/ZrO_2 as 24, 12 and 6. Specifications of PLA and zirconia contents for the synthesis of PLA/ZrO_2 composites are shown in Table 1.

Table 1 — Specifications of PLA and zirconia contents for the synthesis of PLA/ZrO_2 samples

Sample	PLA (± 0.05), g	ZrO_2 (± 0.05), g	PLA/ZrO_2
PLA/ZrO_2 6 %-6	6	1	6
PLA/ZrO_2 6 %-12	6	0.50	12
PLA/ZrO_2 6 %-24	6	0.25	24
PLA/ZrO_2 8 %-6	8	1.33	6
PLA/ZrO_2 8 %-12	8	0.66	12
PLA/ZrO_2 8 %-24	8	0.33	24
PLA/ZrO_2 10 %-6	10	1.66	6
PLA/ZrO_2 10 %-12	10	0.83	12
PLA/ZrO_2 10 %-24	10	0.41	24

Fibrous spun scaffolds were produced via AJS process from PLA and PLA/ZrO_2 polymeric solutions. In all cases, the polymeric solution was placed in a commercially available airbrush TC4176 with a 0.3 mm nozzle diameter and with gravitational feed cup. To synthesize the fibrous scaffolds, 30 mL of each polymeric solution was used. The airbrush was connected to a pressurized argon tank (CAS number 7740-37 concentration > 99 %, PRAXAIR, México) and for fibrous deposition, a pressure of 30 psi with a 21 cm distance from the nozzle to the target was maintained constantly. The deposition time was taken as 30 min at a rate of 1 mL/min.

2.4 Measurements

The X-ray diffractograms were obtained using a D-5000 Siemens diffractometer and Cu Kα radiation (1.5406×10^{-10} m). The diffraction pattern and image of zirconium oxide nanocrystals were obtained using a transmission electronic microscope (TEM) (JEOL model JEM-1200EX) with accelerating voltage of 110 kV and a focal distance (L) of 100 cm. The surface morphology of the PLA and PLA/ZrO_2 fibres scaffolds was observed by scanning electron microscopy (FE-SEM, JSM-7800F.JEOL). The diameters of the fibres were determined by using the Image J software. The mechanical tests were carried out according to ASTM-D1708 using Universal testing machine (Instron model 1125), with a crosshead speed of 10 mm/min at 20 °C and 50 % RH. The data were derived from stress-elongation curve by Instron 55R interface of IX Series Software 8.30.00. For the nitrogen adsorption and desorption test, a model machine Minisorp II brand Bel-Japan was used. The adsorption temperature was 77 K, the saturated vapor pressure was 81.741 kPa and the adsorption cross-sectional surface was 0.162 nm^2. The thermogravimetric analysis of samples was done

using a TGA Q500 equipment (TA Instruments, USA). Platinum 100 µL baskets were tared before automatically to weigh 8 mg of the sample, to be analyzed. The samples were heated up steadily at a rate of 10 °C/min from 20 °C to 1000 °C. The data were analyzed using TGA software (Universal V4.5A TA Instruments). Differential scanning calorimetry measurements were carried out using a Q20 DSC equipment (TA Instruments, USA). Four milligrams of each sample were weighed and prepared in standard DSC aluminum capsules. Initial temperature was set at 25 °C following an isothermal period of 3 min. Thermal scan was programmed with increments of 10 °C/min until a final temperature of 240 °C was reached. The data were analyzed using DSC software (Universal V4.5A TA Instruments), identifying melting points (T_m) and glass transition temperature (T_g). Pure 6 wt% PLA was used as control. The degree of crystallinity (χ_c) was calculated by the following equation:

$$\chi_c = \frac{\Delta H_m}{\Delta H_0} \times 100$$

where ΔH_0 corresponds to the fusion heat of 100 % crystalline PLA (93.6 J/g) [37, 38].

Contact angle measurements were made using a model Ramé Hart Inc. goniometer. Four sessile drops with a volume of 4 mL were handled for each sample. Falling drop and volume were controlled by means of drop volume control software. A camera (model Rainbow CS with a lens L 3.3-8 mm, Japan) was applied to record, and Image J software was utilized to analyze the drops. The wettability was calculated using the Young's equation ($\mu = \cos\theta$) and it was determined whether the surfaces are hydrophobic or hydrophilic according to the established criteria[39].

3 Results and Discussion

3.1 X-Ray Diffraction Study

The X-ray diffractogram for zirconia nanoparticles is shown in Fig. 1(a). Polycrystalline structure with some diffraction peaks is observed. According to the JCPDS card No. 03-065-0461, the main peaks (the most intense) correspond to zirconia in cubic phase, and these are (111) at 30.40°, (200) at 35.25°, (220) at 50.71° and (311) at 60.28°. Also some diffraction peaks corresponding to monoclinic phase are identified using the JCPDS card No. 00-037-1484; these peaks are (-111) at 28.18°, (111) at 31.47°, (200) at 34.16° and (022) at 50.12°. The average size of ZrO_2 crystals is estimated with the Scherrer formula[40]. The angle (2θ) 50.50° is used to obtain a 7 nm average crystal size, and with the angle (2θ) 28.37° an average size of 15 nm is obtained. Figure 1(b) exhibits the diffractogram of PLA fibres for PLA concentrations of 6, 8 and 10 wt% and PLA/ZrO_2 concentrations of 6, 12 and 24 wt%. Although in PLA, diffractograms are not found to show well-defined diffraction peaks — a typical behavior of an amorphous structure, the wide band at 2θ = 10° - 25° can be considered an indicative of a semicrystalline structure because the majority of PLA diffraction peaks are (or should be) in that range, and the fact that the PLA is not crystalline is observed directly from AJS method[33]. Besides that, PLA/ZrO_2 diffractograms show the wide band at 2θ = 10° - 25°, corresponding to PLA semicrystalline structure and the same diffraction peaks of ZrO_2 as shown in Fig. 1(a). This, as expected, shows increase in intensity as

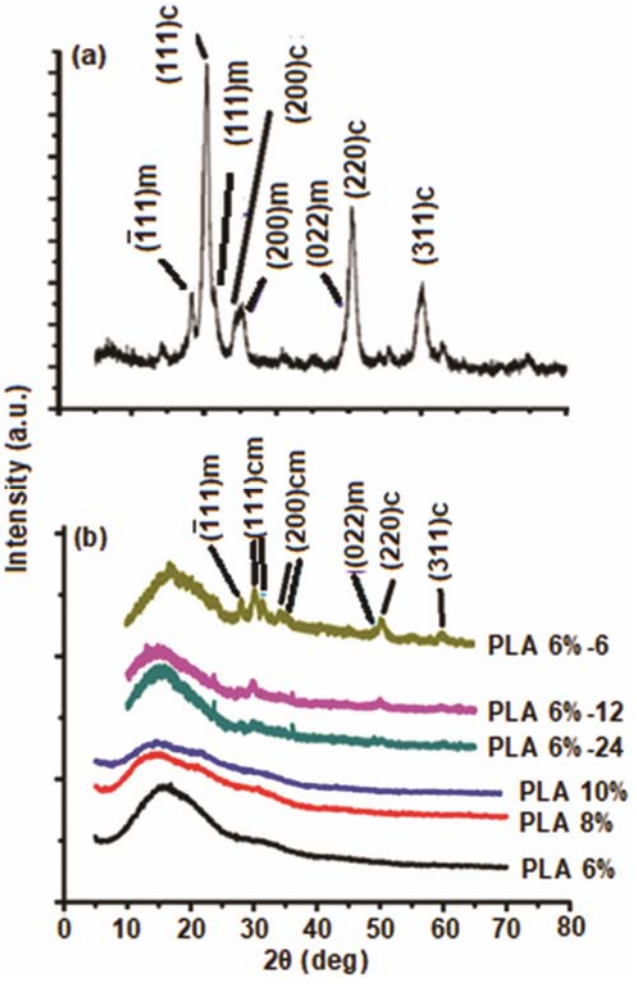

Fig. 1 — XRD diffractograms of (a) ZrO_2 and (b) PLA 6, 8 & 10 %wt and PLA/ZrO_2 6 %wt-6, 12 & 24

the concentration of zirconia increases. X-ray diffractograms are also obtained for the other two concentrations (8 and 10 wt%) of PLA/ZrO_2 composite, but are not discussed in this study because they are very similar to those obtained for samples with 6 wt% concentration, varying only the intensity of the zirconia peaks.

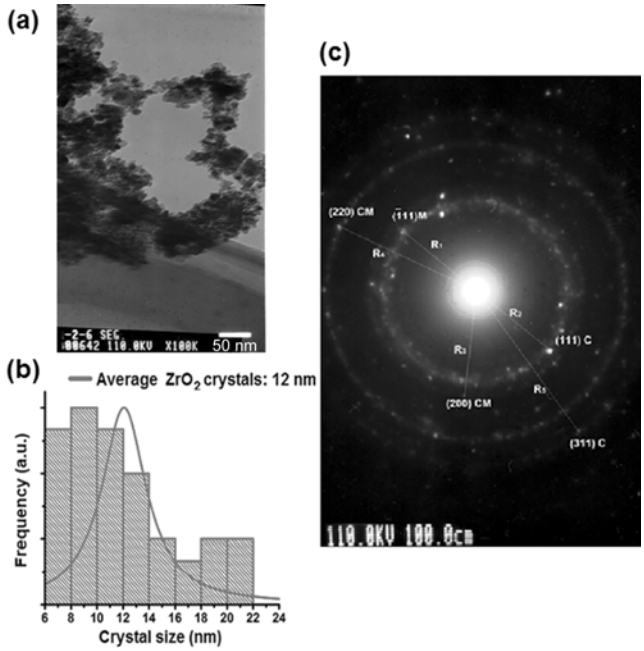

Fig. 2 — (a) TEM micrograph of ZrO_2, (b) average ZrO_2 crystals, and (c) electron difraction partern of ZrO_2 NPs

3.2 Transmission and SEM Study

The results obtained from TEM for ZrO_2 nanoparticles are shown in Fig. 2. Figure 2(a) shows presence of a large number of crystals with an average size of 12 nm, which is similar to the crystal size estimated by Scherrer formula. The average crystal size is also shown in the histogram [Fig. 2(b)]. In Fig. 2(c), concentric rings are observed which corresponds to polycrystalline structure. Using the zirconium oxide cards JCPDS No. 03-065-0461 (cubic) and 00-037-1484 (monoclinic) and measuring the radius, it is determined that the first ring corresponds to $(-111)_M$, the second to $(111)_C$, the third to $(200)_{CM}$, the fourth to $(220)_{CM}$ and the fifth to $(311)_C$. As can be seen, the results from TEM corroborate with the findings from XRD measurements, that is, the powder obtained by hydrothermal synthesis corresponds to polycrystalline zirconia in cubic and monoclinic phases with average crystals size less than 15 nm.

Figure 3 shows SEM micrographs of the PLA fibres at the concentrations of 6 (**a**), 8 (**b**) and 10 (**c**) wt% and the composite PLA/ZrO_2 at concentration of 10 wt%-6 (**d**), 12 (**e**) and 24 (**f**). The micrographs corresponding to PLA fibres show formation of fibres with a random distribution, non-porous structure and a variable fibre diameter. Besides that, in the micrographs of composites PLA/ZrO_2 10 wt%-6, 12 and 24, a number of beads are observed, which can be

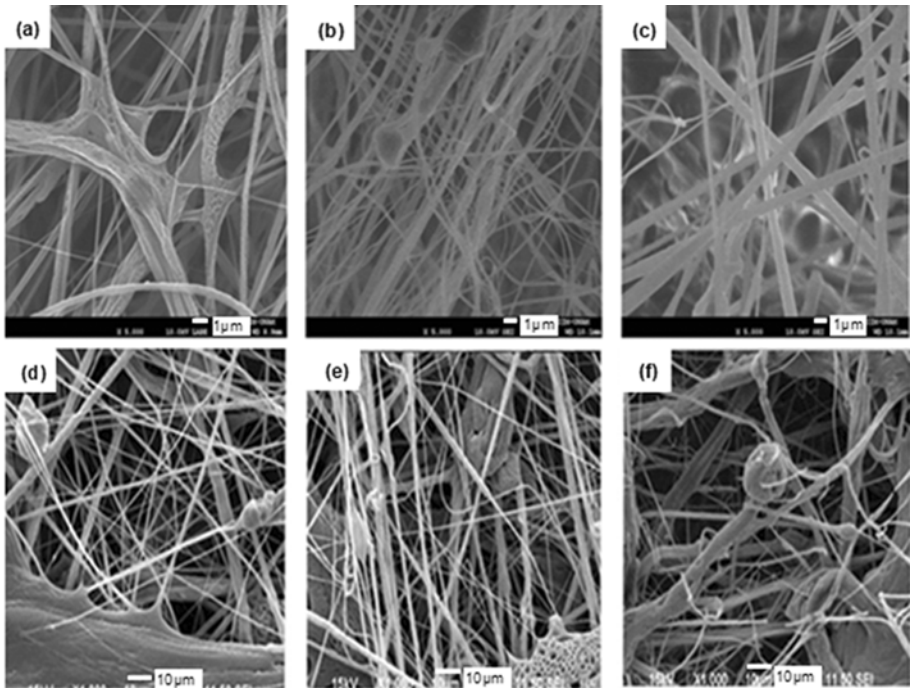

Fig. 3 — SEM micrographs of PLA (a) 6, (b) 8 & (c) 10 %wt, and PLA/ZrO_2 10 %wt composites (d) 6, (e) 12 & (f) 24

attributed to the fact that the zirconia particles are within the PLA and the fibres are agglomerate around the ZrO_2 nanoparticles, creating beads. The average diameter size of PLA fibres and PLA/ZrO_2 composites are shown in Table 2. The average diameter sizes of PLA 6 wt% fibres are found 242 nm, PLA 8 wt% 329 nm and PLA 10 wt% 480 nm. It is clear that the diameter size increases with increase in PLA concentration[34]. Moreover, in all cases, it is observed that the diameter size increases as more zirconia is incorporated. In the case of PLA/ZrO_2 6 wt% composites, the diameters increase from 548 nm (6%-24) to 721 nm (6%-6), for PLA/ZrO_2 8 wt% composites the diameters increase from 577 nm (8%-24) to 780 nm (8%-6) and for PLA/ZrO_2 10 wt% composites the diameters increase from 586 nm (10%-24) to 1070 nm (10%-6) being the last one with biggest diameter size. From the above results, it can be observed that the incorporation of ZrO_2 particles results in an increase in the diameter of PLA/ZrO_2 fibres.

3.3 Mechanical Properties and Wettability

The results on mechanical properties and wettability for PLA fibres and PLA/ZrO_2 composites are shown in Table 2, which are obtained by averaging the values of 4 specimens. The data is analyzed using the Tukey and ANOVA tests. In the case of Young's module, least significant difference (LSD) of 55.9 MPa is obtained. According to that, there is no significant difference in the Young's modulus for PLA 6, 8 and 10 %wt, that is, the concentration percentage does not influence the Young's modulus values. However, as it is expected, there is significant difference among the samples PLA 8 %wt and PLA/ZrO_2 8wt%-6, 12, 24; and samples PLA 10 %wt and PLA/ZrO_2 10 %wt-6, 12, 24. Although in the case of the sample PLA 6 %wt, there is a difference in the sample PLA/ZrO_2 6 %wt-6. It can be said that, in general, the ZrO_2 increases the value of Young's modulus. LSD, is obtained at stress results 0.42 MPa and elongation 0.4 mm. According to that, the PLA concentration percentage influences the stress and the elongation, because there is significant difference among samples with PLA 6, 8 and 10 %wt. From Table 2, it is noticeable that the zirconia nanoparticles make harder and less flexible PLA fibres. For sample PLA 6 %wt, stress increases more than double and breaking elongation decreases by half. In samples PLA 8 and 10 %wt, breaking elongation decreases by approximately one third and stress increases four times.

PLA fibres at the concentration of 6, 8 and 10 %wt show contact angles in the range of 124° - 127° corresponding to negative wettability, and consequently the liquid does not wet fibres surface, showing hydrophobicity. As it can be seen, zirconia decreases the contact angle but it should not be less than 90°. Therefore, the composites PLA/ZrO_2 continue to have negative wettability which keeps them having hydrophobic surfaces. This can be explained by the fact that, as seen in the SEM study, ZrO_2 widens the diameters of the fibres and in some parts overlaps them, but without changing the fibrous morphology.

Figure 4 illustrates the stress-elongation curve and contact angle obtained for sample PLA 6 %wt and composites PLA/ZrO_2 6 %wt-6, 12, 24. In the curves, it is observed that as the amount of zirconium oxide increases, the stress that fibres support also increases, but the elongation is reduced.

Table 2 – Fibre diameter, tensile properties and wettability of PLA and PLA/ZrO_2

Sample	Average fibre diameter	Young´s modulus	Breaking elongation	Stress	Contact angle (θ)	Wettability
	nm	MPa	mm	MPa	deg	μ
PLA 6%	242	44.2	2.17	1.45	124.920°	-0.572
PLA/ZrO_2 6%-6	721	152.1	1.00	3.63	108.100°	-0.311
PLA/ ZrO_2 6%-12	642	83.2	1.66	1.97	101.984°	-0.210
PLA/ ZrO_2 6%-24	548	60.9	1.17	1.74	93.878°	-0.070
PLA 8%	329	6.9	3.50	0.69	126.679°	-0.597
PLA/ ZrO_2 8%-6	780	168.0	0.95	2.12	125.222°	-0.577
PLA/ ZrO_2 8%-12	657	165.6	1.08	2.98	119.981°	-0.500
PLA/ZrO_2 8%-24	577	114.1	1.00	2.08	102.082°	-0.209
PLA 10%	480	16.1	2.66	0.71	126.243°	-0.591
PLA/ ZrO_2 10%-6	1070	173.0	0.92	3.10	124.216°	-0.562
PLA/ ZrO_2 10%-12	679	130.3	1.05	2.33	122.938°	-0.544
PLA/ ZrO_2 10%-24	586	111.1	1.66	2.83	119.699°	-0.495

3.4 Nitrogen Adsorption and Desorption Isotherms Study

Figures 5(a) – (c) show the nitrogen adsorption and desorption isotherms for zirconia nanoparticles, PLA fibres 6, 8 and 10 wt% and composites PLA/ZrO_2 10 wt%-6, 12, 24 respectively. For ZrO_2 nanoparticles and for PLA/ZrO_2 composites, a hysteresis of type H2 is observed, which indicates the possible existence of mesopores in the materials. By contrast, the adsorption and desorption isotherms for PLA fibres match and, hence hysteresis is not there; for that reason PLA fibres do not have mesoporous behavior. The total specific surface area for ZrO_2 (a_s, BET) is 101 m^2g^{-1}, which is greater than the values already reported[41]. For fibres of PLA 6, 8 and 10 %wt a surface area of 0.91, 0.74 and 0.54 m^2g^{-1} respectively is observed. In the case of PLA/ZrO_2 composites, the specific surface area obtained is 0.58, 1.14 and 2.06 m^2g^{-1} for the samples PLA/ZrO_2 10 %wt-24, 12 and 6 respectively. It is immediately noticed that the addition of ZrO_2 increases the value of BET surface area for PLA/ZrO_2 composites. Due to the hysteresis existence, BJH model is used on zirconia nanoparticles and PLA/ZrO_2 composites[42], to obtain their respective pore distribution curves [Figures 5(d) and 5(e)]. In Fig. 5 (d), the mesoporous distribution peak (r_p, peak area) is found at 4.05 nm, and the pore diameter is 8.1 nm, which is very close to the pore size obtained by BET (7.1 nm). It can be observed from Fig. 5(e) that pore sizes are less than 5 nm, which indicates that composites are mesoporous materials and the mesoporosity is due to the inclusion of ZrO_2 nanoparticles.

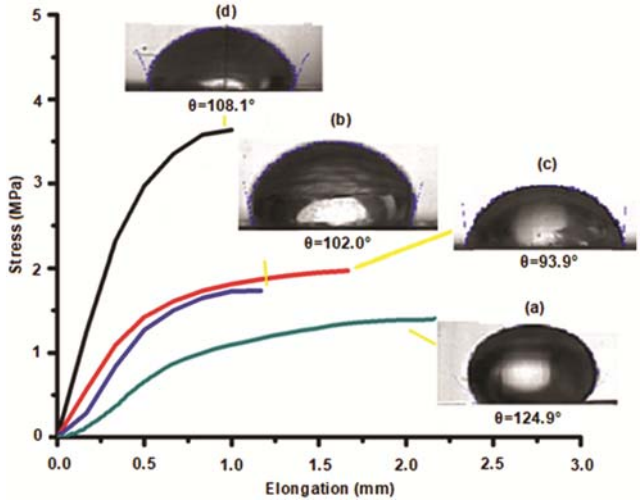

Fig. 4 — Stress-elongation curves of (a) PLA 6 %wt, (b) PLA/ZrO_2 6 %wt-24, (c) PLA/ZrO_2 6 %wt-12 and (d) PLA/ZrO_2 6 %wt-6

3.5 DSC and TGA Study

Table 3 shows glass transition temperature (T_g), melting temperature (T_m), fusion heat and degree of crystallinity acquired by DSC. For fibres of PLA 6, 8 and 10 %wt, it is observed that the concentration does not affect the glass transition temperature and melting temperature, since the values practically match with a difference of less than 1 °C for glass transition temperature and less than 0.5 °C for melting temperature. However, on adding zirconia, there is a

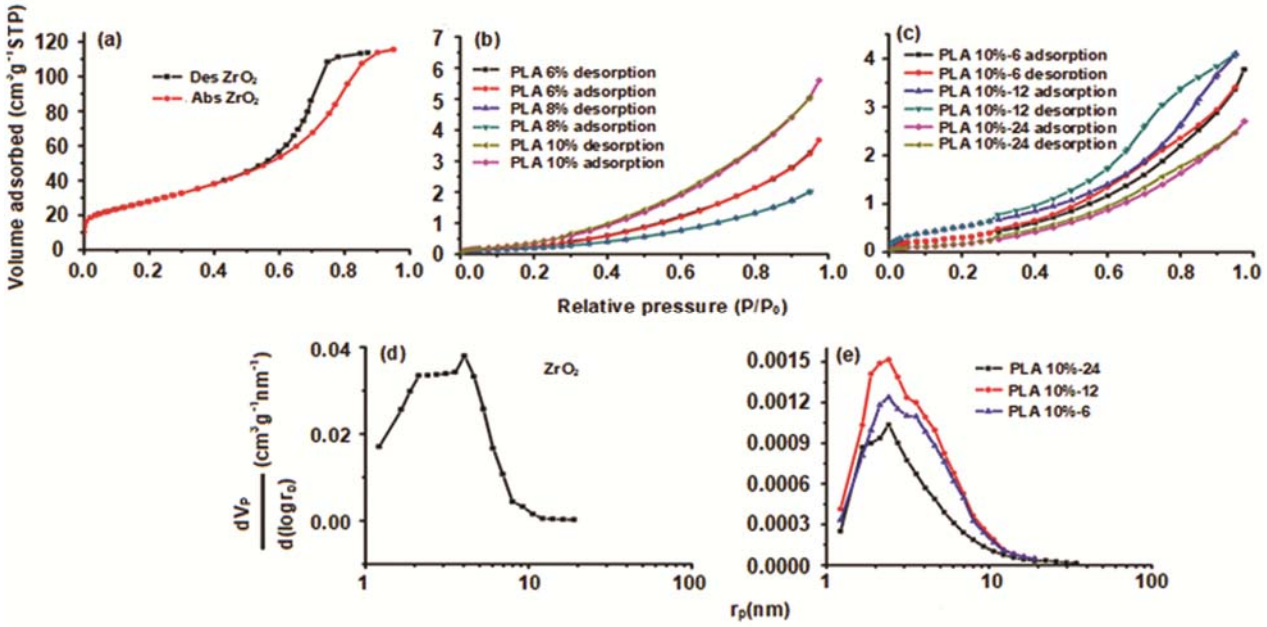

Fig. 5 — Nitrogen adsorption-desorption isotherms of (a) ZrO_2 nanoparticles, (b) PLA 6, 8 and 10 %wt, (c) PLA/ZrO_2 10 %wt-6,12 and 24. Distribution mesoporous size curve of (d) ZrO_2 nanoparticles and (e) PLA/ZrO_2 10 %wt-6,12 and 24

Table 3 – First-order transitions and crystallization parameters of samples

Sample	T_g, °C	T_m, °C	ΔHm, J/g	χ_C, %
PLA 6%	62.06	152.26	20.02	21.39
PLA/ZrO_2 6%-24	66.04	152.70	24.64	26.32
PLA/ZrO_2 6%-12	65.89	152.72	22.16	23.67
PLA/ZrO_2 6%-6	66.05	152.94	23.81	25.43
PLA 8%	62.14	151.94	20.47	21.87
PLA/ZrO_2 8%-24	65.19	151.67	23.15	24.73
PLA/ZrO_2 8%-12	65.16	152.46	24.72	26.41
PLA/ZrO_2 8%-6	66.12	152.90	27.82	29.72
PLA 10%	61.15	151.94	21.88	23.38
PLA/ZrO_2 10%-24	65.53	151.51	25.90	27.67
PLA/ZrO_2 10%-12	65.37	150.10	23.07	24.65
PLA/ZrO_2 10%-6	66.22	152.66	23.40	25.00

small increase in T_g (~ 4 °C) and T_m (<1 °C). The largest increase occurs in the ΔHm, which is reflected directly in composites having a higher crystallinity than in pure fibres. For instance, comparing the PLA 8%wt with composite PLA/ZrO_2 8%wt -6, it is observed that the glass transition temperature increases from 62.14°C for sample PLA 8%wt to 66.12 °C corresponding to sample PLA/ZrO_2 8 %wt-6. The melting temperature for PLA 8%wt is obtained as 151.94 °C and it reaches a maximum value of 152.90 °C for sample PLA/ZrO_2 8 %wt-6. Moreover, the most significant change occurs in the fusion heat going from 20.47 J/g to 27.82 J/g, which is reflected in an increase in the crystallinity from 21.87 % to 29.72 %. This increase is due to the crystallinity of zirconia, and that there is no significant difference in the T_g and T_m for PLA fibres. The findings for PLA/ZrO_2 composites are related to the amount of zirconia used.

Figure 6(a) exhibits the thermal decomposition curve for ZrO_2 nanoparticles. The loss in mass that occurs below 150 °C is because of the dehydration of the sample. From 150 °C to 700 °C, a 2 %wt loss is detected due to the decomposition of the hydroxyl groups. The loss of mass between 700 °C and 900 °C is due to the decomposition of absorbed water, and in this range the maximum loss of weight per unit temperature is observed at 775 °C. Therefore, zirconia has a good thermal stability for temperatures below 1000 °C.

The thermal decomposition curves for PLA 8% wt and PLA 8 % wt - 24 are shown in Figs 6(b) and (c) respectively. It is observed that the behavior of fibres and composite is very similar. In the case of fibres, the thermal decomposition occurs in the range 316°-367 °C, while for composite the range

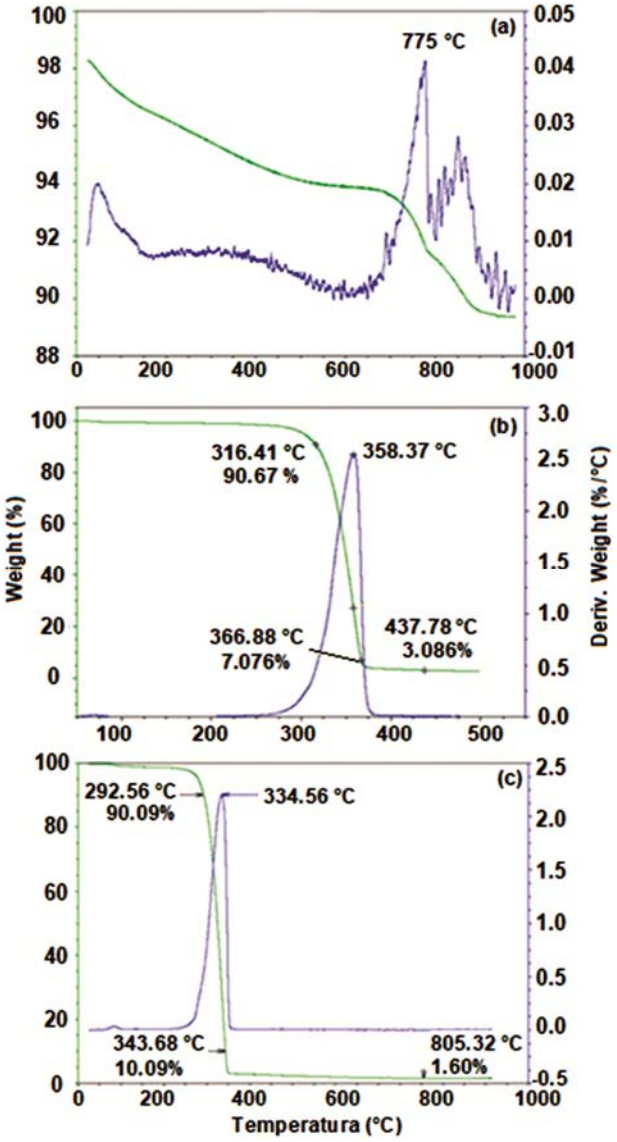

Fig. 6 — TGA curves of (a) ZrO_2 nanoparticles, (b) PLA 8 %wt fibres and (c) PLA/ZrO_2 8 %wt-24

decreases from 292°-344 °C. Although there is a small decrease in the decomposition interval, both fibres and composites have a thermal stability up to 300 °C. In both cases, the residue is attributed to the char formation from the PLA; however, in the case of composites the residue is also attributed to ZrO_2 NPs.

4 Conclusion

Using the hydrothermal synthesis method, it is possible to synthesize nano-structured, mesoporous and thermally stable ZrO_2 particles, which are used to form PLA/ZrO_2 composites deposited by AJS method. PLA/ZrO_2 composites have a fibrous

morphology with a random distribution. The incorporation of ZrO_2 nanoparticles results in an increase in the diameter of fibres, reaching a maximum value of 1 μm. Moreover, ZrO_2 nanoparticles increase the hardness of fibres, but affect the flexibility; stress being the maximum for composite (up to four times that of PLA fibres). The most important result obtained is that, composites are mesoporous materials and the mesoporosity is due to ZrO_2 nanoparticles, suggesting that PLA/ZrO_2 composite may be used as biomaterial. Besides that, ZrO_2 nanoparticles duplicated BET area, which can facilitate the interaction of composite with other compounds. Neither hydrophobic behavior of fibres nor thermal properties are influenced by ZrO_2 nanoparticles.

Acknowledgement

Authors are thankful to the Omar Novelo, Raul Reyes, Adriana Tejeda, Eliezer Hernández, Carlos Flores, Francisco Gómez and Gerardo Cedillo from IIM-UNAM, for their technical assistance. Two authors (EAAO) and (RMCO) want to thank CONACYT (No.1 486933 and No.2 487111) for their doctoral scholarship during the course of this study. The financial support from DGAPA-UNAM: PAPIIT IT203618 is gratefully acknowledged.

References

1 Ortiz-Islas E, López T, Navarrete J, Bokhimi X & Gómez R, *J Molecular Catalysis A: Chem*, 228 **(**2005) 345.
2 Liu X Y, Huang A P, Ding C X & Chu P K, *Biomater*, 27 (2006) 3904.
3 Piconi C & Maccauro G, *Biomater*, C 20 (1999) 1.
4 Wattanasiriwech D, Wattanasiriwech S & Stevens R, *Mater Res Bull*, 41 (2006) 1437.
5 Hannink R H J, Kelly P M & Muddle B C, *J Am Ceram Soc*, 83 (2000) 461.
6 Subbarao E C & Maiti H S, *Adv Ceram*, 24 (1988) 731.
7 Due-Hansen J, Boghosian S, Kustov A, Fristrup P, Tsilomelekis G, Ståhl K, Christensen CH & Fehrmann R, *J Catalysis*, 251 (2007) 459.
8 Pratima R, Kaushik A S, Chavhan P M, Maheshwari S N & Malhotra B D, *Electrochem Comm*, 11 (2009) 2272.
9 Luo Z A, Xiao J Z & Xia F, *Trans Nonferrous Met Soc*, 16 (2006) 82.
10 Kumari L, Du L G, Li W Z, Vennila R S, Saxena S K & Wang D Z, *Ceram Int*, 35 (2009) 2401.
11 Chen H & Ding C X, *Surf Coat Technol*, 150 (2002) 31.
12 Trivinho-Strixino F, Guimarães F E G & Pereira E C, *Chem Phys Lett*, 461 (2008) 82.
13 Wright P K & Evans A G, *Sol St Mater Sci*, 4 (1999) 255.
14 French R H, Glass S J, Ohuchi F S, Xu Y N & Ching W Y, *Phys Rev B*, 49 (1994) 5133.
15 Gao P, Meng L J, dos Santos M P, Teixeira V & Andritschky M, *Thin Solid Films*, 377-378 (2000) 32.
16 Tuan W H, Chen J R & Ho Ch J, *Ceram Int*, 34 (2008) 2129.
17 Schmidt T, Mennig M & Schmidt H, *J Am Ceram Soc*, 90 (2007) 1401.
18 Štefanć II, Musić S, Štefanić G & Gajović A, *J Mol Struct*, 480-481 (1999) 621.
19 Liang J, Jiang X, Liu G, Deng Z, Zhuang J, Li F & Li Y, *Mater Res Bull*, 38 (2003) 161.
20 Wang L, Cai K F, Wang Y Y, Yin J L, Li H & Zhou C W, *Ceram Int*, 35 (2009) 2499.
21 Liang J H, Deng Z X, Jiang X, Li F L & Li Y D, *Inorganic Chem*, 41 (2002) 3602.
22 Kumari L, Li W & Wang D, *Nanotech*, 19 (2008) 321.
23 Huang Ch, Guo R, Tang Z & Zhang Z, *J Am Ceram Soc*, 88 (2005) 1651.
24 Khollam Y B H, Deshpande A S, Patil A J, Potdar H S, Desphande S B & Date S K, *Mater Chem Phys*, 71 (2001) 235.
25 Dell'Agli G & Mascolo G, *J Eur Ceram Soc*, 20 (2000) 139.
26 Sagadevan S, Podder J & Das I, *J Mater Sci Mater Electron*, 27 (2016) 5622.
27 Behbahani A, Rowshanzamir S & Esmaeilifar A, *Proc Eng*, 42 (2012) 908.
28 Dharmaraj N, Kim C H & Kim H Y, *Synt React Inorg Met-Org NanoMet Chem*, 36 (2006) 29.
29 Ahmed S, Yasin M, Ibrahim O, Mohamed A, Yousef A & Barakat N A M, *Royal Soc Chem Adv*, 7 (2017) 4616.
30 Ibrahim Mohamed M A, Dao V D, Barakat N A M, Ahmed S, Yasin M, Yousef A & Choi H S, *J Coll Inter Sci*, 476 (2016) 9.
31 Li F, Kang Z, Huang X & Zhang G J, *Ceram Inter*, 40 (2014) 10137.
32 Zimmermann M V G, Brambilla V C, Brandalise R N & Zattera A J, *Mater Res*, 16 (2013) 1266.
33 Huaa Z, Niea M, Liub X & Wanga Q, *J Macromol Sci Part B: Physics*, 56 (2017) 306.
34 Abdal-hay A, Barakat N A M & Lim J K, *Sci Adv Mater*, 4 (2012) 1.
35 Santos D, Correia C O, Silva D M, Gomes P S, Fernandez M H, Santos J D & Secandas V, *Mat Sci Eng*, C 75 (2017) 1184.
36 Corcione C E, Gervaso F, Scalera F, Montagna F, Sannino A & Maffezzoli A, *J Appl Polym Sci*, 134 (2017) 44656.
37 Lim L T, Auras R & Rubino M, *Prog Polym Sci*, 33 (2008) 820.
38 Liu X, Wang T, Chow L C, Yang M & Mitchell J W, *Int J Polym Sci* (2014) doi:10.1155/2014/827028.
39 Abdal-hay A, Sheikh F A & Lim J K, *Colloids Surf B: Biointerfaces*, 102 (2013) 635.
40 Kumar D & Pandey K N, *Indian J Chem Technol*, 24 (2017) 153.
41 Klimova T, Gutierrez O, Lizama L & Amezcua J, *Micropor Mesopor Mater*, 133 (2010) 91.
42 Vargas-Osorio Z, Chanes-Cuevas O A, Pérez-Soria A, García-Hipólito M, Alvarez-Fregoso O, Alvarez-Pérez M A, *Phys Status Solidi C*, (2016). DOI 10.1002/pssc.201600099.